UNIVERSITYOF BIRMINGHAM

Research at Birmingham

Transport of spatial squeezing through an optical waveguide

Hordell, Joshua; Benedicto Orenes, Daniel; Petrov, Plamen; Kowalczyk, Anna; Barontini, Giovanni; Boyer, Vincent

Document Version
Publisher's PDF, also known as Version of record

Link to publication on Research at Birmingham portal

Transport of spatial squeezing through an optical waveguide

JOSHUA HORDELL, DANIEL BENEDICTO-ORENES, PLAMEN G. PETROV,* ANNA U. KOWALCZYK, GIOVANNI BARONTINI, AND VINCENT BOYER

Midlands Ultracold Atom Research Centre, School of Physics and Astronomy, University of Birmingham, Edgbaston, Birmingham B15 2TT, UK
*p.g.petrov@bham.ac.uk

Abstract: Multi-core optical fibers are readily used in endoscopic devices to transmit classical images. As an extension to the quantum domain, we study the transmission of the spatial quantum fluctuations of light through a conduit made of the ordered packing of thousands of fibers. Starting from twin beams that are correlated in their local intensity fluctuations, we show that, in the limit of a high density of constituent fiber cores, the intensity-difference squeezing present in arbitrary matching regions of the beams is preserved when one of the beams is sent through the conduit. The capability of using fiber bundles to transport quantum information encoded in the spatial degrees of freedom could bring guided-light technology to the emergent field of quantum imaging.

References and links

1. M. Peev, C. Pacher, R. Alleaume, C. Barreiro, J. Bouda, W. Boxleitner, T. Debuisschert, E. Diamanti, M. Dianati, J. F. Dynes, S. Fasel, S. Fossier, M. Furst, J.-D. Gautier, O. Gay, N. Gisin, P. Grangier, A. Happe, Y. Hasani, M. Hentschel, H. Hubel, G. Humer, T. Langer, M. Legre, R. Lieger, J. Lodewyck, T. Lorunser, N. Lutkenhaus, A. Marhold, T. Matyus, O. Maurhart, L. Monat, S. Nauerth, J.-B. Page, A. Poppe, E. Querasser, G. Ribordy, S. Robyr, L. Salvail, A. W. Sharpe, A. J. Shields, D. Stucki, M. Suda, C. Tamas, T. Themel, R. T. Thew, Y. Thoma, A. Treiber, P. Trinkler, R. Tualle-Brouri, F. Vannel, N. Walenta, H. Weier, H. Weinfurter, I. Wimberger, Z. L. Yuan, H. Zbinden, and A. Zeilinger, "The SECOQC quantum key distribution network in Vienna," New. J. Phys, **11**(2), 075001 (2009).
2. V. Subramanian and Krish Ragunath, "Advanced Endoscopic Imaging: A Review of Commercially Available Technologies," Clinical Gastroenterology and Hepatology, **12**(3), 368–376 (2014).
3. W. Löffler, T. G. Euser, E. R. Eliel, M. Scharrer, P. St. J Russell, and J. P. Woerdman, "Fiber Transport of Spatially Entangled Photons," Phys. Rev. Lett. **106**(24), 240505 (2011).
4. Y. Kang, J. Ko, S. M. Lee, S-K Choi, B. Y. Kim, and H. S. Park, "Measurement of the Entanglement between Photonic Spatial Modes in Optical Fibers," Phys. Rev. Lett. **109**(2), 020502 (2012).
5. H. J. Lee, S-K Choi, and H. S. Park, "Experimental Demonstration of Four-Dimensional Photonic Spatial Entanglement between Multi-core Optical Fibres," Sci. Rep. **7**(1), 4302 (2017).
6. Y. Israel, R. Tenne, D. Oron, and Y. Silberberg, "Quantum correlation enhanced super-resolution localization microscopy enabled by a fibre bundle camera," Nature Communications **8**(1), 14786 (2017).
7. G. Brida, M. Genovese, and I. Ruo-Berchera, "Experimental realization of sub-shot-noise quantum imaging," Nat. Photon. **4**(1), 227–230 (2010).
8. V. Boyer, A. M. Marino, and P. D. Lett, "Generation of Spatially Broadband Twin Beams for Quantum Imaging," Phys. Rev. Lett. **100**(14), 143601 (2008).
9. A. Kumar, H. Nunley, and A. M. Marino, "Observation of spatial quantum correlations in the macroscopic regime," Phys. Rev. A **95**(5), 053849 (2017).
10. M. A. Taylor, J. Janousek, V. Daria, J. Knittel, B. Hage, H-A. Bachor, and W. P. Bowen, "Experimental realization of sub-shot-noise quantum imaging," Nat. Photon. **7**(1), 229–233 (2013).
11. Z. Y. Ou, S. F. Pereira, H. J. Kimble, and K. C. Peng, "Realization of the Einstein-Podolsky-Rosen paradox for continuous variables," Phys. Rev. Lett. **68**(25), 3663–3666 (1992).
12. C. F. McCormick, V. Boyer, E. Arimondo, and P. D. Lett, "Strong relative intensity squeezing by four-wave mixing in rubidium vapor," Opt. Lett. **32**(2), 178–180 (2007).

13. E. Brambilla, A. Gatti, M. Bache, and L. A. Lugiato, "Simultaneous near-field and far-field spatial quantum correlations in the high-gain regime of parametric down-conversion," Phys. Rev. A **69**(2), 023802 (2004).
14. This a transverse coherence length and the only one we will refer to in the rest of the paper.
15. E. D. Lopaeva, I. Ruo Berchera, I. P. Degiovanni, S Olivares, G. Brida, and M. Genovese, "Experimental Realization of Quantum Illumination," Phys. Rev. Lett. **110**(15), 153503 (2013).
16. M. A. Taylor, J. Janousek, V. Daria, J Knittel, B. Hage, H-A Bachor, and W. P. Bowen, "Subdiffraction-Limited Quantum Imaging within a Living Cell," Phys. Rev. X **4**(1), 011017 (2014).
17. A. Yariv, "Optical Electronics," Saunders College Publishing, (1991).
18. M. W. Holtfrerich, and A. M. Marino, "Control of the size of the coherence area in entangled twin beams," Phys. Rev. A, **93**(6), 063821 (2016).
19. C. S. Embrey, M. T. Turnbull, P. G. Petrov, and V. Boyer, "Observation of Localized Multi-Spatial-Mode Quadrature Squeezing," Phys. Rev. X **5**(3), 031004 (2015).
20. A. Perperidis, H. E. Parker, A. Karam-Eldaly, Y. Altmann, K. Dhaliwal, R. R. Thomson, M. G. Tanner, and S. McLaughlin, "Characterization and modelling of inter-core coupling in coherent fiber bundles," Opt. Express **25**(10), 11932–11953 (2017).
21. V. Boyer, A. M. Marino, R. C. Pooser, and P. D. Lett, "Entangled Images from Four-Wave Mixing," Science **321**(5888), 544–547 (2008).
22. M. D. Reid, "Demonstration of the Einstein-Podolsky-Rosen paradox using nondegenerate parametric amplification," Phys. Rev. A **40**(2), 913–923 (1989).
23. A. Porat, E. Ravn Andresen, H. Rigneault, D. Oron, S. Gigan, and O. Katz, "Widefield lensless imaging through a fiber bundle via speckle correlations," Opt. Express **24**(15), 16835–16855 (2016).
24. A. Fertman and D. Yelin, "Image transmission through an optical fiber using real-time modal phase restoration," J. Opt. Soc. Am. B **30**(1), 149–157 (2013).
25. T. Cizmar and K. Dholakia, "Exploiting multimode waveguides for pure fibre-based imaging," Nature Communications **3**(1), 1027 (2012).
26. M. I. Kolobov, and C. Fabre, "Quantum Limits on Optical Resolution," Phys. Rev. Lett., **85**(18), 3789–3792 (2000).
27. C. Caves and D. Crouch, "Quantum wideband traveling-wave analysis of a degenerate parametric amplifier," J. Opt. Soc. Am. B 4, 1535-1545 (1987).

1. Introduction

The ubiquity of optical communications is due in large part to the advent of the optical fiber, which allows for flexible and efficient routing of light-encoded information. Used as serial channels, single fibers have also been shown to be effective to transport quantum information, for instance in commercial quantum key distribution systems [1]. At the same time, fiber technology has progressed to support the transmission of full images in fiber bundles, e.g. in endoscopic devices [2], and the question arises whether one can extend this property of parallel transmission of information to the quantum domain. In these imaging applications, the information of a classical image is contained in the local amplitude of the light field incident on the input face of the bundle. The ordered packing of the fibers in the bundle guaranties the conservation of the light intensity distribution across the beam profile, therefore the image is preserved during the propagation and reappears on the output face of the bundle. In the quantum domain, this will be equivalent to ensuring that the quantum correlations associated with the intensity fluctuations of an arbitrary spatial feature, that is to say an input transverse mode, are reproduced on the output of the guide in the exact same mode.

Previous experimental research in the guiding of the spatial quantum states of light has been essentially limited to the single-photon subspace. For instance, guided transport and full state tomography has been demonstrated for pairs of photons spatially entangled over two spatial modes in multimode fibers [3,4], and for photons spatially entangled over up to four spatial modes in multicore fibers [5]. Beyond this small number of spatial modes, only the spatially-resolved detection of photons, that is to say an intensity measurement, has been demonstrated, typically by combining a fiber bundle to an ensemble of single-photon detectors. In this manner, the temporal nonclassical statistics of spatially resolved photons emitted by scattered emitters was observed over a bundle of 15 fibers [6]. Such spatially resolved guiding of single photons, or photons belonging to correlated pairs, could be useful to channel illumination or signal in low-light-level quantum imaging applications [7]. The interest in transporting quantum states of light for imaging

however, goes beyond these low fluxes of photons. Macroscopic states of light are better suited to the imaging of hard-to-see objects, e.g. very weakly absorbing objects, because at the quantum noise limit (QNL) a larger probing intensity provides a better signal-to-noise ratio. In this context, bright two-mode squeezed states of light, containing arbitrary mean numbers of photons, have been shown to display local intensity correlations below the shot noise limit both in the frequency [8] and time domains [9], and are therefore good candidates for practical quantum imaging. This is particularly true for those applications where the illumination intensity cannot be arbitrarily increased due to the existence of a damage threshold [10], and where squeezing the quantum fluctuations of light are the only solution to increase the signal to noise ratio.

Here we address the issue of the transport of a bright illumination with a fiber bundle while preserving local intensity fluctuations at the quantum level. Starting from a two-mode squeezed state [11], that is to say a pair of continuous-variable (CV) entangled light beams which display intensity and phase quantum correlations of their random spatial fluctuations, we transport one of the beams through the bundle and show that the spatial intensity correlations with the other beam are preserved, as evidenced by the presence of local intensity-difference squeezing after the transport.

2. Experimental setup

The two-mode squeezed state is created using a phase-insensitive optical amplifier. Our amplifier is based on four-wave-mixing (4WM) in a hot ^{85}Rb vapor in a double-lambda configuration [12], as described in the Appendix 5.1. The process is efficient enough to realize a nonlinear single-pass gain of a few units without the need of an enhancement cavity. Because of the finite length of this traveling-wave amplifier, the strict phase-matching condition is relaxed and the resulting two-mode squeezed state is intrinsically spatially multimode. This means that the twin beams, probe and conjugate, are entangled across multiple spatial modes, or regions [8]. In particular, matching pairs of locales in the cross-sections of the beams are correlated. In the plane of the cell, referred to as the near field, these regions are mapped onto each other because probe and conjugate correlated fluctuations are born in the same location. In the far field these regions are symmetrically placed about the pump propagation axis due to transverse momentum conservation. Diffraction associated with the propagation over the finite length of the cell leads to a minimum transverse size over which correlations can be observed, the coherence area [13], with an associate coherence length [14]. As the coherence area is substantially smaller than the beams size, a large number of modes, typically a few tens, are independently correlated. This unique feature makes the twin beams a useful resource for imaging with sensitivity [15] or resolution [16] beyond the shot-noise limit, and efficiently guiding of the beams would make these applications more practical.

We chose to focus on intensity correlations in the near field. To this effect, we separate the twin beams and we image their nonlinear interaction region onto individual "measurement" planes, as shown in Fig. 1. In these planes, identical locations on the twin beams display quantum intensity correlations which we aim to preserve after transport in a fiber bundle.

The fiber bundle itself is a rigid conduit, designed to transmit (coherently) optical images with a resolution given by the fiber size. It is 15cm long and contains 5×10^4 fibers with diameter of 12μm tightly packed into a equilateral triangular lattice. Fig. 2(a) shows an image of the output face of the conduit injected with a Gaussian beam of diameter smaller than the conduit diameter, and reveals the packing structure. The incomplete filling leads to an overall transmission of around 30%, primarily determined by the ratio of the fiber core total area to the conduit input face area, but also by partial reflection on the faces of the conduit. The large core size of the fibers makes them multimode for near-infrared optical wavelengths, as evidenced by the irregularity in the shapes of the light beams coming out of the individual fibers.

The discretization introduced by the finite fiber size sets a natural length scale for the smaller
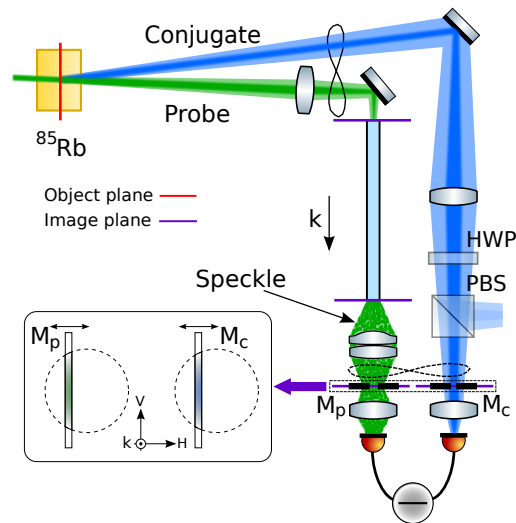
Fig. 1. **Experimental setup.** The conjugate and probe beams are generated via 4WM in the ^{85}Rb cell. The probe light in the object plane, i.e. the plane at the position of the cell, where the correlations are created, is imaged onto the input face of the conduit. The probe light emerging from the output face of the conduit is imaged onto the probe slit on the measurement plane (M_p) using a high numerical aperture optical system. The conjugate is directly imaged onto the conjugate slit on the measurement plane (M_c). The conjugate slit is translated in horizontal (H) and vertical (V) directions perpendicular to the direction of propagation $\mathbf{k}$, for every position of the probe slit as shown in the inset. The polarizing beamsplitter (PBS) and the half-wave plate (HWP) in the path of the conjugate provide a tunable loss for the channel to balance the beams intensities in the case where the probe is sent through the conduit. The lightly colored paths depict the geometric propagation of the quantum fluctuations whereas the densely colored paths depict the Gaussian propagation of the bright probe and conjugate beams. The pump beam is not shown for clarity. The figures of eight indicate CV entanglement (solid line) and quantum intensity correlations (dashed line).

spatial details that can be transmitted by the conduit. At the quantum level, one can expect that only fluctuations of spatial modes substantially larger than the inter-fiber spacing will be accurately transmitted across the guide. We therefore image the beam on the input face of the conduit in such a way that the fiber size is much smaller than the estimated coherence area, as shown in Fig. 2(a). This means that all the scales of correlations present in the system should be successfully transmitted. In this configuration, the capacity of the bundle is much higher than the number of squeezed modes in the transmitted light. Because of the structure and the continuity of the spatial squeezing, independent correlated areas do not have sharp boundaries. They overlap and cannot be separated to be fed to individual cores of the bundle.

The loss of probe light due to the finite transmission of the conduit induces a mismatch between the probe and conjugate fluctuations at the balanced photodetector, which can be corrected by introducing an adequate level of attenuation on the conjugate beam, as shown in Fig. 1. Since the effect of loss on a beam of light is to mix vacuum noise to the fluctuations of the beam, the measured squeezing after loss is less than the squeezing before loss. Therefore the initial degree of squeezing (3.0 dB) and the level of attenuation of the conjugate (25%) are chosen to maximize the level of squeezing seen after the conduit. The details of the procedure are given in the Appendix 5.2.

Although the fiber bundle conserves the coarse distribution of intensity between the input and
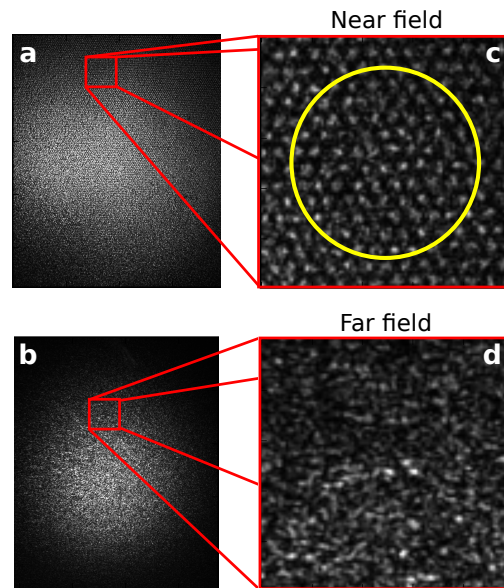
Fig. 2. **Images of the probe beam after the conduit. a,b** Images of the near- and far-field beam patterns after the conduit, showing the Gaussian intensity envelope. **c,d** Selected magnified regions across the profiles in **a** and **b**, respectively. In **c**, in the near-field, the characteristic pattern coming from the hexagonal lattice of constituent fibers can be clearly seen at the output face of the conduit. The lattice spacing is about 12 μm. Since the fibers are multimode, the emerging mode shape is random across the fiber lattice. The enclosed circular area represents the estimated coherence area of the process. In **d**, in the far field the fiber lattice pattern is transformed into a speckle pattern as the light from every fiber acquires a random phase.

the output, modal dispersion, i.e. group velocity dispersion for different spatial modes within each fiber [17] as well as differential dispersion between the fibers, leads to the scrambling of the phase of the output field on a length scale of the order of the size of the fiber cores. As a consequence of this wavefront distortion, the output beam is diffracted following the large numerical aperture (0.55) of the constituent fibers and produces in the far field a speckle pattern, shown in Fig. 2(b), that is very different from the Gaussian mode of the input beam. Therefore the input and output intensity distributions only match on the input and output faces, and faithful transmission of intensity fluctuation distributions puts stringent requirements on the accuracy of the imaging of the plane of interest onto the input face of the conduit. Similarly, the output plane has to be accurately imaged onto the measurement plane. Because of the strong diffraction, the collection optics requires a high numerical aperture (0.5) and has to be accurately placed due to the resulting very short depth of field as described in Appendix 5.3.

Note that because the coherence length is larger than the constituent fiber size, the angular aperture associated with the coherence length is smaller than the numerical aperture of both the fibers and the coupling optics. This ensures that the intensity fluctuations of interest are efficiently coupled to the conduit.

In practice, we test the spatial correlations by selecting small regions on the measurement planes with two movable slits, one on the probe beam and one on the conjugate beam (Fig. 1). The partial powers transmitted through the slits are detected by the separate photodiodes of a balanced photodetector which forms the subtraction of the photocurrents. The noise of the photocurrent difference is measured with a spectrum analyzer, with settings given in Appendix

5.4, and recording the intensity-difference noise as a function of the position of the slits allows us to map the spatial intensity correlations between probe and conjugate. Selecting correlated regions leads to reduced noise below the QNL, whereas mismatched positions produce excess noise associated with phase-insensitive optical amplification. We perform the experiment twice. Firstly, we characterize the spatial correlations generated by the 4WM alone. Secondly, we measure the same spatial correlations after sending the probe beam through the conduit, as shown in Fig. 1.

The slits are set up on pair of translation stages and their width is set to be of the order of the coherence length. While it is possible to accurately evaluate the coherence length [18], we adopt here a more straightforward methodology which consists in selecting the smallest widths of the slits for which we still observe a visible amount of squeezing. Indeed, reducing the slits sizes increases the share of the spatial frequency spectra of the transmission functions of the slits which lie outside the spatial bandwidth of the 4WM process and corresponds to transmitted modes in a vacuum state. If this fraction of the spectrum dominates, the measured noise will tend to the QNL. Note that the spatial spectra associated with the gate-shaped transmission function of the slits always contain high spatial frequencies that lie outside the 4WM spatial bandwidth, which is given by the coherence length. It is therefore expected that selecting correlated regions with slits will always generate reduced measured squeezing. Experimentally the slits are set to ≈15 % of the beams widths and provide an overestimate of the coherence length [19], theoretically estimated to be around 120 μm which is about 8 % of the beams size. After the width is selected, the slits are scanned across the span of the beams, scanning over the conjugate for each region across the probe.

3. Results and discussion

The noise recorded by the balanced detector for each pair of positions of the slits is shown in Fig. 3. A reduction in the intensity-difference noise from the baseline defined by the amplification excess noise, and down below the QNL, is observed when the slits positions match, that is to say when they are identical inside the probe and conjugate beams. The excess amplification noise due to the 4WM, between 1.5dB and 4dB above the QNL, is evident when the slits positions do not match.

Comparing the data with and without the bundle, it is apparent that, apart from a reduction of the overall level of squeezing from −3dB to −1.5dB due to the finite transmission of the device (see Appendix 5.2), the conduit preserves the spatial properties of the quantum state of the light, here the intensity quantum fluctuations. As expected, the spatial resolution of the conduit is better than the coherence length of the beam profile. Indeed the fiber size is 10 times smaller than the coherence length of the transmitted quantum field, which, as estimated by the width of the narrowest trough in Fig. 3(d) is of the order of 100 μm. The exact shape of the noise dips is the result of a combination of the slits transfer function and the coherence profile. The width of the dips can therefore be used to estimate trends of the relative size of the coherence area with respect to the beam sizes. For a fixed slit width, a wider noise dip implies a larger coherence length. In order to gauge the effect of the conduit on the spatial frequency bandwidth of the correlations, we consider the width of the squeezing troughs, κ, relative to the Gaussian beam diameter. In the case of transmission through the conduit, κ is found to be 0.32 and 0.29, for horizontal and vertical scans respectively. In the case of free space propagation, κ is 0.27 and 0.20, respectively.

The comparison between the values of κ with and without the conduit shows that the spatial bandwidth of the spatial correlations is largely preserved during transport. The small loss of spatial resolution can be attributed to a combination of imperfections in the imaging system and conduit behavior. Firstly, the very small depth of field of the high-numerical aperture imaging system, which is required to efficiently collect the light after the conduit, could result in an approximate imaging of the output face of the conduit on the slit. This works in combination
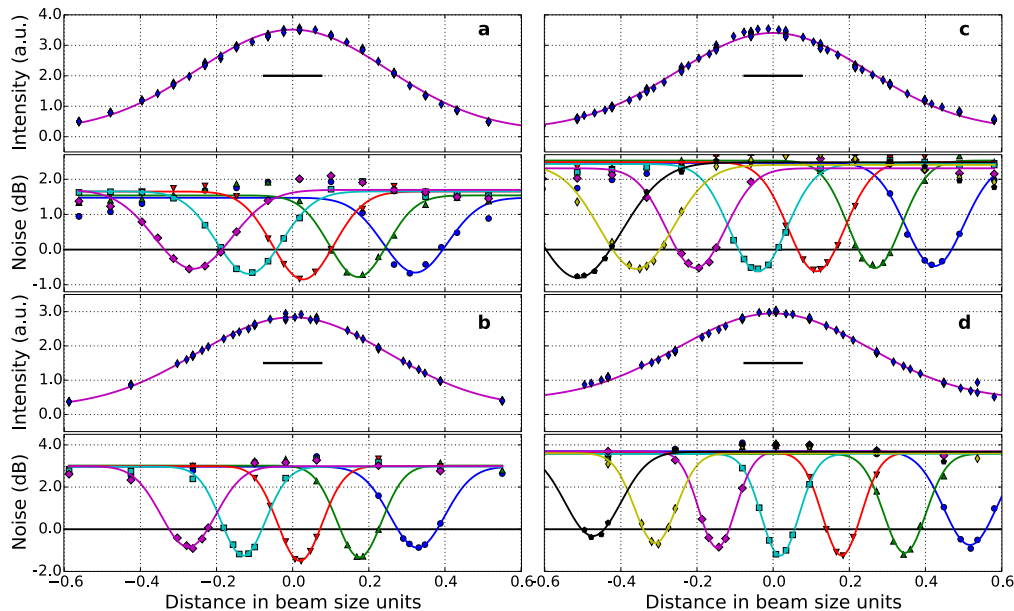
Fig. 3. **Scanning noise data relative to shot noise.** The measurement procedure is done by scanning the slit position on the conjugate beam for fixed positions of the slit on the probe beam. The result is a single dip in the detected noise for each scan. The scanning is done in both horizontal **a,b** and vertical **c,d** directions for the cases where the conduit is inserted in the probe beam path in **a,c**, and when it is not present **b,d**. The top graph in each figure is the fitted intensity profile of the conjugate beam. The noise dips are fitted using Gaussians and the black solid line at 0 dB represents the shot noise. The bar in each beam profile graph denotes the slit size. The excess amplification noise, observed when the slits positions do not match, is larger at the center of the gain medium, where the Gaussian pump beam profile peaks and the gain is the largest. The intensity profile of the conjugate beam is given in arbitrary units (a.u.). No electronic noise or other technical noise have been subtracted from the data.

with the spherical aberrations of the optical system. Secondly, the conduit itself has a small but not negligible cross-talk between fibers [20], which leads to the smearing of the correlations over adjacent correlated regions, resulting in larger width of the troughs.

The two-mode squeezed state generated by the 4WM process nominally displays phase-sum squeezing which, together with the intensity-difference squeezing, results in continuous-variable entanglement [21, 22]. Phase scrambling by the conduit prevents us from directly measuring phase correlations, however phase randomization due to modal dispersion is to be understood with respect to an external reference. Indeed, phase information can still be transmitted as long as a bright coherent carrier is also transmitted so as to serve as a local phase reference, as it is done in this experiment by using a bright beam. The beam emerging from the conduit should display phase fluctuations locally correlated with the phase fluctuations of the other twin beam. Measuring such correlations would require a local oscillator with a wavefront which matches the wavefront of the light on the output face of the conduit. Phase and amplitude control of the local oscillator with a spatial resolution better than the fiber array resolution would be a formidable yet feasible task.

Another solution to the issue of wavefront distortion is direct control of modal dispersion, so that the transmitted beam emerges from the conduit with a flat wavefront. Simply using single-mode fibers as the constituents of the bundle can avoid modal dispersion within individual

fibers, but controlling or correcting for the differential dispersion between the fibers is much harder. Nonetheless there has been progress in real time compensation of modal dispersion to perform classical imaging through single multimode guides or fibers [23–25]. Improving substantially on the spatial resolution of these techniques may lead to the possibility of guiding and preserving the full quantum state of the electromagnetic field, thereby extending the work of Ref. [3] to larger numbers of spatial modes and arbitrary photon numbers.

4. Conclusion

We have demonstrated that spatial quantum intensity correlations, in the form of localized intensity-difference squeezing, can be transported through a fiber bundle. Our work provides initial steps toward the realization of practical quantum enhancement in imaging applications where the shot noise is a limitation and where light guiding would provide additional convenience. For instance, the efficient delivery of intensity-squeezed light would trivially produce images with better signal-to-noise ratio, and multi-spatial-mode squeezed illumination would also lead to better resolution in certain super-resolution schemes [26]. Our experiment uses a standard commercially available conduit, however improved performance could be obtained with a purpose-build device made of single mode fibers for a reduced distortion of the wavefront, more fibers for improved spatial resolution, and optimized packing for increased transmission. Additionally, realizing active phase control would extend the method presented here to the effective guiding of massively parallel entanglement, with possible use in parallel quantum communication links.

5. Appendix

5.1. Four-wave-mixing

The quantum correlations are generated using a non-degenerate 4WM process in a hot ^{85}Rb atomic vapor in a double-lambda configuration [12]. A strong 795 nm pump beam (700 mW) and a weak seed beam (130 μW) intersect at a small angle of $\sim$ 6 mrad into a 12 mm-long vapor cell heated to $\gtrsim$ 100°C. The probe beam is derived from the pump beam via an AOM in a double-pass configuration driven at a frequency of 1.5 GHz, half the ground state hyperfine splitting. The pump and the probe are resonant with a two-photon Raman transition between the hyperfine ground states, with a detuning of $\sim$ 800 MHz to the blue of the $F = 2 \rightarrow F'$ and $F = 3 \rightarrow F'$ transitions, respectively.

The 4WM process corresponds to the transfer of an atom from the $F = 3$ hyperfine ground state to the $F = 2$ hyperfine ground state and back to the initial state. In the process the atom consumes two pump photons and emits one probe photon as well as one conjugate photon at a frequency $\sim$ 6 GHz higher than the probe frequency and located symmetrically with respect to the pump beam axis [12]. The hot atomic vapor acts as a phase-insensitive amplifier for the probe with a single-pass gain of 1.5-2. This is enough to amplify the probe and generate a conjugate beam in a traveling-wave configuration, that is to say without the use of a cavity. The bandwidth of the nonlinear process is about 20 MHz.

5.2. Losses

The conduit has a transmission of around 30%. This leads to an imbalance between the probe and conjugate signals and a sub-optimal subtraction of the common amplification noise. For practical reasons, we use a perfectly balanced photodetector, which subtracts the photocurrent before trans-amplification. This prevents us from applying a different trans-amplification gain on both signals in order to re-balance them. We show here that even with balanced detection, the problem can be partially mitigated by choosing a correct combination of optical gain and attenuation on the conjugate beam path, and that squeezing can be observed after transport in the conduit.
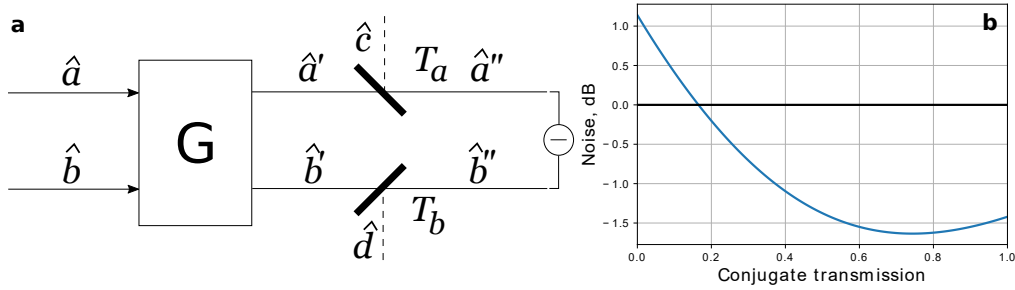
Fig. 4. **Theoretical model of losses in the experiment. a.** The FWM medium has a gain of G. The input probe and conjugate annihilation operators are depicted by $\hat{a}$ and $\hat{b}$. After the amplification the operators are $\hat{a}'$ and $\hat{b}'$ and after mixing vacuum fields $\hat{c}$ and $\hat{d}$ at beamsplitters with transmission T_a and T_b the operators are transformed to $\hat{a}''$ and $\hat{b}''$. **b.** Optimization of conjugate transmission. The probe transmission is 0.3 and the maximum squeezing for a gain of 1.5 can be seen to happen at transmission of the conjugate of 0.75. The solid black line is the shot noise.

Losses on both beam paths, including finite transmission by the conduit, losses on lenses and mirrors, balancing beamsplitter on the conjugate and finite quantum efficiency of the detector, are modelled by a single beamsplitter on each beam, whose effect is to attenuate the beam and inject vacuum noise [27]. The four-wave mixing amplification and loss model is presented in Fig. 4(a). The field operators at detection are:

$$\begin{aligned}
\hat{a}'' &= \sqrt{GT_a}\,\hat{a} - \sqrt{(G-1)T_a}\,\hat{b}^\dagger + \sqrt{1-T_a}\,\hat{c} \\
\hat{b}'' &= -\sqrt{(G-1)T_b}\,\hat{a}^\dagger + \sqrt{GT_b}\,\hat{b} + \sqrt{1-T_b}\,\hat{d},
\end{aligned} \tag{1}$$

where $\hat{a}$ is the annihilation operator of the input probe field, $\hat{b}$ is the same for input conjugate field, $\hat{c}$ and $\hat{d}$ are the loss annihilation operators coupled to the probe and conjugate fields via beamsplitters with transmission T_a and T_b, and G is the four-wave-mixing gain. This leads to the variance in the differential number of detected photons $\hat{n}_- = \hat{n}''_a - \hat{n}''_b$ for a coherent state $|\alpha\rangle$ on input a and a vacuum $|0\rangle$ on input b:

$$\begin{aligned}
\langle(\Delta\hat{n}_-)^2\rangle &= \{[GT_a - T_b(G-1)]^2 + G(G-1)(T_b - T_a)^2 \\
&+ GT_a(1-T_a) + (G-1)T_b(1-T_b)\}|\alpha|^2.
\end{aligned} \tag{2}$$

The shot noise is given by the mean number of photons of the probe and conjugate at the detector $\langle\hat{n}_+\rangle = \hat{n}''_a + \hat{n}''_b$ and can be written as

$$\langle\hat{n}_+\rangle = [GT_a + (G-1)T_b]|\alpha|^2. \tag{3}$$

Finally, the amount of squeezing is

$$\frac{\langle(\Delta\hat{n}_-)^2\rangle}{\langle\hat{n}_+\rangle}. \tag{4}$$

It is possible to maximize the amount of *detected* squeezing, that is to say the to minimize the amount of intensity difference noise relative to shot noise [Eq. (4)] in both the gain G and the conjugate transmission T_b. For an overall probe transmission $T_a = 0.3$, the optimum values are found to be $G = 1.3$ and $T_b = 1$, resulting in a theoretical -1.65 dB of squeezing. The squeezing varies very softly with these parameters and in practice we choose a gain $G \approx 1.5$ at the centre of the pump beam and a transmission $T_b = 0.75$. This corresponds to a theoretical squeezing of 3.0 dB below shot noise before the conduit and 1.63 dB after it [see Fig. 4(b)]. A value close

to this amount of squeezing is indeed observed when measuring the squeezing on the intensity difference of the whole beams (about -1.5 dB). The measured degree of squeezing when using the slits is lower than the whole beam value however, both with and without the conduit. This is due to the fact that the transmission function of the slits lays partially outside the spatial bandwidth of the 4WM process, both because the slits width is of the order of the coherence length, and because their transmission functions contains high spatial frequencies due to their sharp edges. Furthermore, optical aberrations may contribute to reduced measured correlations.

5.3. Optical imaging

To reveal the intensity spatial correlations produced locally in the gain medium, the median plane in the vapor cell, the near field, must be imaged on the selection slits. When the conduit is introduced in the probe path, the near field must in addition be imaged on the input facet of the conduit. Direct imaging of the near field on the conduit or the slits is done with a single long-focal-length lens of 250 mm. Imaging of the exit facet of the conduit on the probe selection slit is done with high-numerical-aperture doublet made of 8 mm focal length aspheric lens and a 16 mm focal length lens.

5.4. Noise detection

The light going through the slits is detected by a balanced photodetector with quantum efficiency of 95%. For practical reasons, the gain is identical for both photodiodes. The trans-amplified differential photocurrent is analyzed with a spectrum analyzer operating at an analyzing frequency of 2 MHz, a resolution bandwidth of 30kHz, and a video bandwidth of 30Hz.

Data availability

The data presented here are available from the University of Birmingham Institutional Research Archive, accessible online at doi: 10.25500/eData.bham.00000173.